Nature Environment and Pollution Technology
An International Quarterly Scientific Journal

p-ISSN: 0972-6268
(Print copies up to 2016)
e-ISSN: 2395-3454

Vol. 21 | No. 3 | pp. 1125-1135 | 2022

Original Research Paper

https://doi.org/10.46488/NEPT.2022.v21i03.017

Open Access Journal

Efficient Adsorptive Performance of Graphene Oxide by Nano Clay

Wenjie Yu, Biao Qian, Beifeng Lv, Haibo Kang†, Ping Jiang, Wei Wang and Na Li
School of Civil Engineering, Shaoxing University, Shaoxing 312000, China
†Corresponding author: Haibo Kang; 18020852079@usx.edu.cn

Nat. Env. & Poll. Tech.
Website: www.neptjournal.com

Received: 30-07-2021
Revised: 26-09-2021
Accepted: 04-10-2021

Key Words:
Adorption
Graphene oxide
Nano clay

ABSTRACT

Research regarding the use of Nano clay to remove toxic GO (Graphene oxide) from wastewater was limited. Through a variety of characterization techniques and methods, the adsorption performance and mechanism of Nano clay for GO were systematically studied. The related effects of solution pH, temperature, adsorbent dose, and GO concentration were studied in detail. The results show that the aggregation and deposition of GO on Nano clay depends on the pH value of the solution and the type and concentration of the electrolyte, and the isotherm data fits well with the Langmuir equation. Under the best conditions (pH=3.0), the maximum removal rate is 97.8% (C_0=60 mg·L^{-1}), and the adsorption capacity is 245.8 mg.g^{-1} (C_0=80 mg.L^{-1}, T=303K, equilibrium time=24 h, m=10 mg). Specifically, the dissolution of Nano clay at a relatively low pH or a high pH value helps the aggregation of GO. The results of this study provide key information for predicting the fate of GO in the land-water transition zone where Nano clay exists.

INTRODUCTION

With many advanced properties of the hydrophilic surface, easy modification, and good dispersion in water (Liu et al. 2019a, 2019b), graphene oxide (GO) has been used in various fields. In view of the increasing production of graphene-based nanomaterials and their incorporation in consumer products, they are likely to be discharged into the sewage treatment plant (Burkart et al. 2015) and further into the environment. When the wastewater is untreated or inadequately treated, the high concentration of GO in the wastewater will threaten the lives of animals and plants on the earth (Chen et al. 2019, Tabish et al. 2017). Although there is no known record of the precise concentration of GO in wastewater treatment plants, some authors have been modeling and testing to find possible concentrations. Chen et al. 2019, Tabish et al. 2017, Gottschalk et al. 2013). Currently, there are many different technologies used to remove GO from sewage. Due to its selectivity, low operating cost, affordability, simple operation, high efficiency, and reusable adsorbent, adsorption technology is considered to be one of the best methods to treat wastewater.

In recent years, many adsorbents have been studied for the removal of GO, such as layered double hydroxides (Wang et al. 2016), and Al_2O_3 (Ren et al. 2014). Other low-cost adsorbents have also been studied. Clay minerals have been proposed as alternative adsorbents for GO. In addition, clay minerals are widely distributed and abundant in soil, which makes them a promising environmental adsorbent for industrial processes (Deng et al. 2017). Due to the widespread existence and availability in soil and sediments, clay has been used as a flocculant and adsorbent for the treatment of suspended particles, pathogenic organisms, and toxic compounds in water (Rozhina et al. 2019). In the past thirty years, the use of clay and clay minerals for water treatment has been extensively studied (Hızal & Yılmazoğu, 2021). Examples of such applications include removing grease from water, building clay linings to intercept organic leachate in waste treatment sites, absorbing heavy metals and destroying endocrine chemicals, and recovering nitrogen from nitrogen-rich wastewater, Therefore, there is greater potential for adsorption of GO using natural clays.

The purpose of this study is to evaluate the potential use of Nano clay as a natural adsorbent for the removal of GO under the same experimental conditions. In the adsorption studies, all the parameters that affect the adsorption were studied, such as the amount of adsorbent, the pH value of the aqueous solution, and the initial concentration of GO.

MATERIALS AND METHODS

Materials

All chemicals (analytical grade) used in the experiment were purchased from Sinopharm Chemical Reagent Co., Ltd. (Shanghai, China). Nano clay was purchased from Hubei Gold Fine Montmorillonite Technology Co., Ltd. (Hubei, China). The content of montmorillonite is greater than 91.27%. The particle size of nano clay is in the range of 1-2 nm, the surface area is in the range of 220-270 $m^2.g^{-1}$ and

the density is in the range of 0.03-0.37 g.cm^{-3}. The graphene oxide aqueous solution was purchased from Suzhou Tanfeng Graphene Technology Co., Ltd. (Jiangsu, China).

Batch Experiments

Removal experiments were carried out in a series of vials with teflon-lined nuts fitted with batch technology. A certain amount of Nano clay (0.01 g) was added to the vial to achieve the required concentration of different ingredients. The required initial pH value (3-10) of the suspension in each vial was adjusted by adding negligible 0.1 mol.L^{-1} NaOH or HCl. The vials containing these mixtures were placed on a horizontal shaker and shook at a constant speed of 220 rpm for 1 hour. Subsequently, the vial was taken out of the shaker and left to stand on a flat surface for 24 hours to allow the aggregates of Nano clay and GO to settle completely. Finally, the residual concentration of GO (Ce (mg.L^{-1})) in the supernatant was determined by a UV-vis spectrophotometer (UV-2550, PerkinElmer) at a wavelength of 221 nm (Wang et al. 2016). Formulas 1-3 were used to calculate the relevant parameters:

$$R\% = \frac{C_0 - C_e}{C_0} \times 100\% \quad \ldots(1)$$

$$q_e = \frac{(C_0 - C_e) \times V}{m} \quad \ldots(2)$$

$$K_d = \frac{Q_e}{C_e} \quad \ldots(3)$$

Where, C_0 (mg.L^{-1}) and C_e (mg.L^{-1}) represent the initial and equilibrium concentrations of GO, and Q_e represents the amount of adsorption.

Characterization

Using CuKα radiation, the crystal structure of the absorbent was detected by an X-ray diffractometer (XRD, Empyrean). The functional groups were identified by Fourier Transform Infrared Spectroscopy (FT-IR, NEXUS), and the scanning range was 400-4000cm^{-1}. Scanning electron microscope (SEM, JSM-6360LV), atomic force microscope (AFM, SPA400), and high-resolution transmission electron microscope (HRTEM, JEM-2100F) were used to study the morphology and element composition of the composite material. X-ray photoelectron spectroscopy (XPS) was performed by a Thermo ESCALAB 250 spectrometer, which applied a focused monochromatic Al Ka X-ray source (hm=1486.6 eV).

RESULTS AND DISCUSSION

Structural and Morphological Characterization

XRD analysis: The assessment of the structures of nano-clay materials is strongly supported by the XRD patterns. The crystalline structures of products were identified with XRD. 2θ values were recorded in the XRD patterns of GO, Nano clay, and Nano clay/GO in the range from 5° to 90°, as shown in Fig. 1. As can be seen from the figure, GO and nano clay have obvious diffraction peaks. The adsorption of Nano clay on GO was evaluated by XRD. After Nano clay adsorbs GO, the diffraction peak structure changes. It can be seen from the figure that after Nano clay adsorbs GO, the characteristic peak of Nano clay still exists, but becomes weaker. A weak peak around the GO (001) one is detected in nano clay/GO, and a small variation in its position can be due to an expansion of the stacking of the GO layer. This shows that Nano clay/GO is a mixture of nano clay and GO. This is because the XRD test only scans the surface of the sample, while GO /nano clay is the sample obtained from the adsorption of GO by nano clay. The XRD results show that the XRD pattern is similar to that of nano

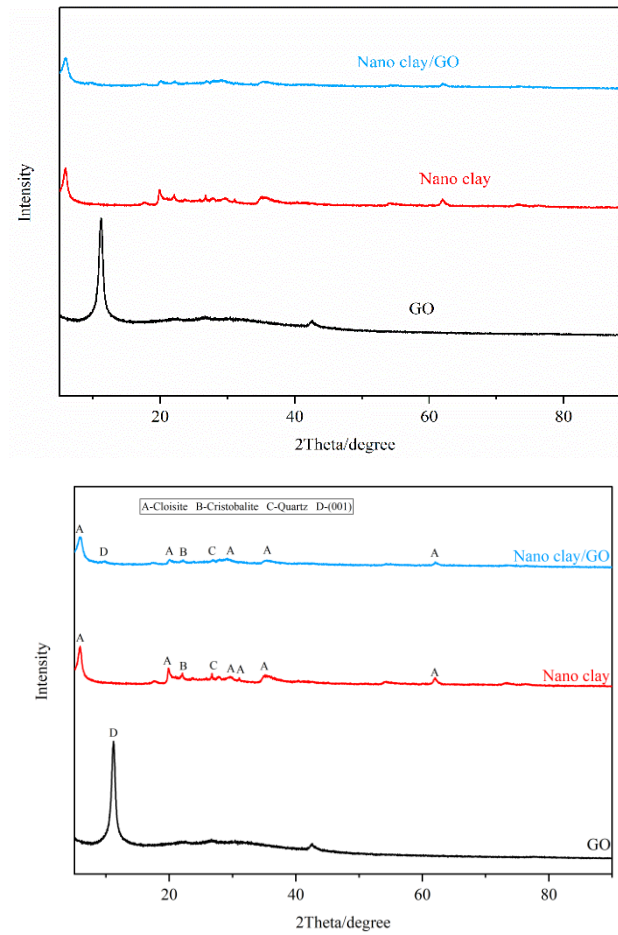

Fig. 1: XRD analysis of GO, Nano clay, and Nano clay/GO. (Adsorption conditions for Nano clay:pH=3, C_0=60 mg.L^{-1}, m=80 mg, T=303K).

clay and cannot be observed to be similar to that of GO. Diffraction peaks indicate that there is a large amount of nano clay on the surface of the sample, and the GO portion in the GO/nano clay is blocked by the nano-clay. The change of structure is beneficial to improve the adsorption capacity of the adsorbent (Yan et al. 2010).

SEM analysis: To investigate the surface morphology and structure distribution before and after GO adsorption with SEM. The morphology and microstructure of the material were analyzed by a scanning electron microscope (SEM). The SEM micrographs of GO, Nano clay, and Nano clay/GO are shown in Fig. 2 (a, b, c). The lamellar structure of GO is visible in the SEM image (Fig. 2a). The porous structure of Nano clay is regarded as a layered structure, with irregular particle shapes, agglomerates of variable size, and sharp edges (Fig. b), which is consistent with earlier reports (Yi et al. 2015). On the other hand, when nano clay adsorbs GO, it can be seen that nano clay is covered with a film similar to GO (Fig. 2c) and GO is distributed on the porous network surface of Nano clay with less stacking, indicating that Nano clay has adsorbed GO.

TEM analysis: The structural evolution of the material preparation process was observed under transmissive electron microscopy, and the morphology and particle diameter of the product before and after adsorption can be further analyzed (Qi et al. 2015). TEM and XRD together are one of the main tools used to determine the dispersion of clay nanoparticles, and the obtained TEM image correlates well with the XRD results (Bae et al. 2009). The structure evolution during the preparation of the material was observed under the transmission electron microscope. GO is a multi-layer folded gauze (Liu et al. 2015) (Fig. 3a). When Nano clay absorbs GO, a layer of black substance is obviously attached to the surface of GO in flake shape, and the wrinkles will be significantly reduced or even disappeared (Fig. 3b), which is consistent with XRD diffraction pattern results and SEM images.

AFM analysis: We use AFM images from different dimensions to characterize micro-morphology evolution in the material preparation process (Zhang et al. 2019). AFM was used to further illustrate the above results. Fig. 4 shows the representative 2D AFM images of GO and Nano clay/GO. The cross-sectional analysis and white lines of the AFM image are shown in Figs. 4b and d. From the evolution of the AFM micromorphology, the thickness of GO measured by AFM shows that all samples exhibit a single layer or double layer, which is consistent with previous research results (Liu et al. 2018). However, as the thickness of Nano clay/GO increases, Nano clay is buried in the GO sheet, indicating that Nano clay successfully adsorbs GO. Representative results of AFM images are consistent with previous XRD, FT-IR, SEM, and TEM analyses.

XPS analysis: XPS was also used to further investigate the

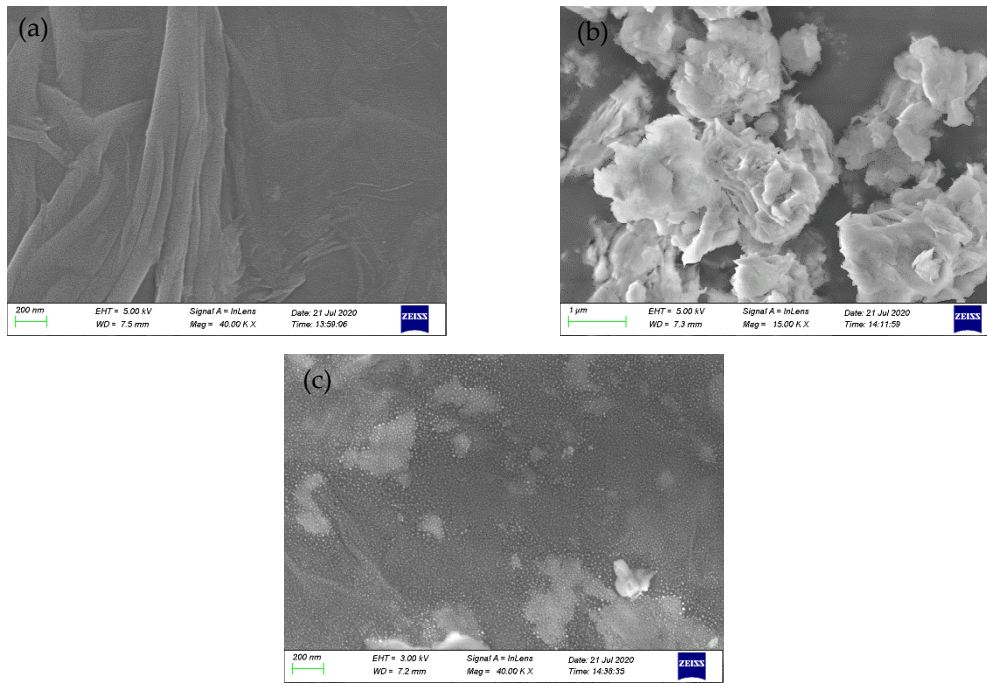

Fig. 2: SEM images of (a) GO, (b) Nano clay, and Nano clay/GO (c). (Adsorption conditions for Nano clay:pH=3, C_0=60 mg.L^{-1}, m=80 mg, T=303K).

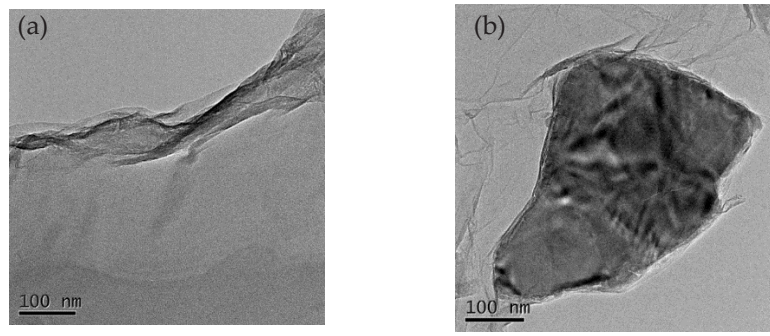

Fig. 3: TEM analysis of GO(a), and Nano clay/GO (b). (Adsorption conditions for Nano clay:pH=3, C_0=60 mg.L^{-1}, m=80 mg, T=303K).

adsorption mechanism. XPS is a surface-sensitive technique for the analysis of the chemical environments of elements. The chemical environment changes of the element in a functional group due to adsorption can be identified through the shift of binding energy in the corresponding XPS spectrum (Ciftyurek et al. 2019). The XPS spectra of Nano clay adsorbing GO are related to the characteristic peaks of C 1s and O 1s in the original GO, respectively. As shown in Fig. 5, various strong peaks can be observed, such as Al 2p, Mg 1s, N 1s, Cl 2p, Cl 1s, O 1s, and C 1s, indicating that the main elements on the surface of the sample are magnesium, aluminum, and oxygen. Compared with the C 1s before GO adsorption, the strength of C 1s after GO adsorption by Nano clay is significantly reduced. From the high-resolution C 1s spectra before GO adsorption, the C 1s spectra can be deconvoluted and integrated into four components, which are about 284.8 eV,

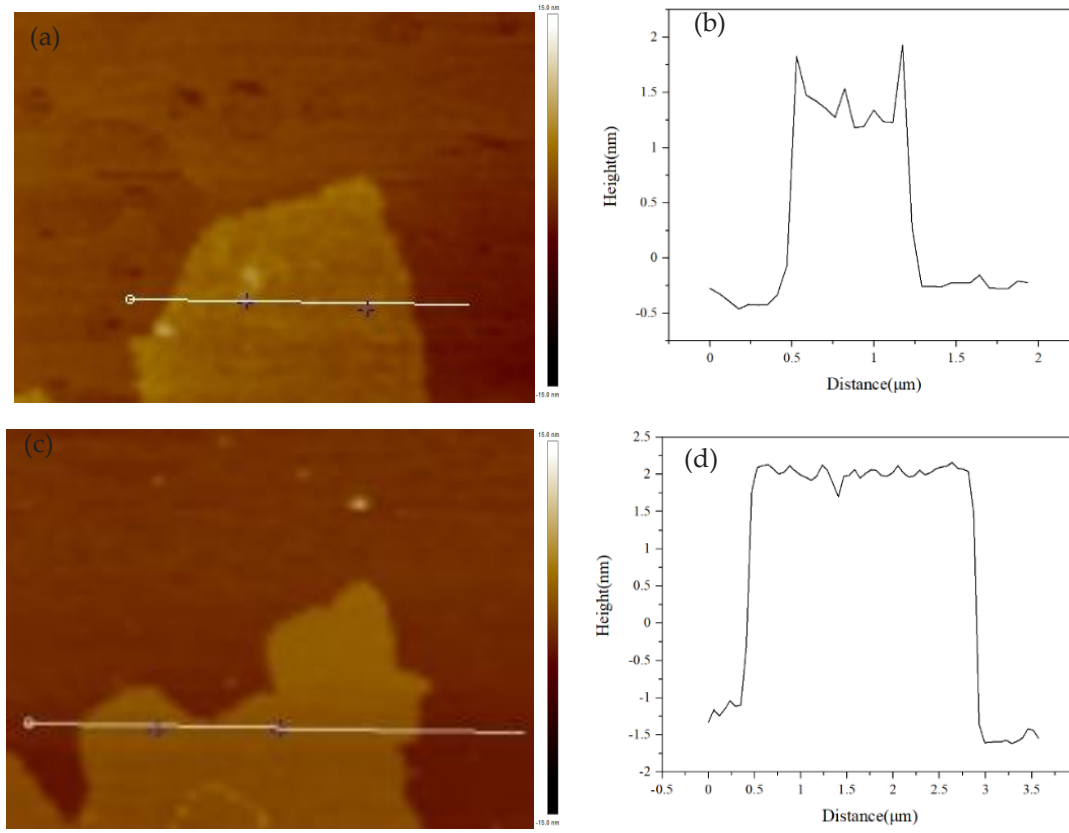

Fig. 4: AFM analysis of GO(a), corresponding height profiles(b), and Nano clay/GO (c), corresponding height profiles (d). (Adsorption conditions for Nano clay: pH=3, C_0=60 mg.L^{-1}, m=80 mg, T=303 K).

286.2 eV, 287.9 eV, and 289.0 eV, respectively (Wen et al. 2013) (Fig. 5 b). The first component with a binding energy of ~284.8 eV is due to non-oxidized ring carbon, and the other three components are due to carbon in C-O (~286.2 eV), carbonyl carbon (C=O, ~287.9 eV) and carboxylic acid Carbon (O-C=O, ~289.0 eV). After GO is adsorbed by Nano clay, C=O disappears, indicating that the adsorption process of GO and Nano clay is carried out by C=O. According to the above analysis, Nano clay can effectively remove GO by adsorbing GO and attaching it to its surface.

Adsorption Performance

pH Effect: The pH value of GO solution is an important parameter for adsorption (E et al. 2020). Fig. 6 illustrates the change in the adsorption capacity of Nano clay on GO when the initial GO concentration is 60 mg.L^{-1}. Visual fitting data shows that in the pH range of 3-10, the adsorption capacity first decreases and then increases, and performs best at pH=3. High surface area and adsorbent functional groups can improve the adsorption efficiency (Naser et al. 2016). As shown in Fig. 6, when pH<5, the adsorption capacity, removal rate and distribution coefficient of Nano clay on GO first decrease with the increase of pH. However, when pH ≥5, the above three indicators are reversed. The increase in pH may be related to the initial pH of GO. It is known that the surface charge of clay in the solution is negative

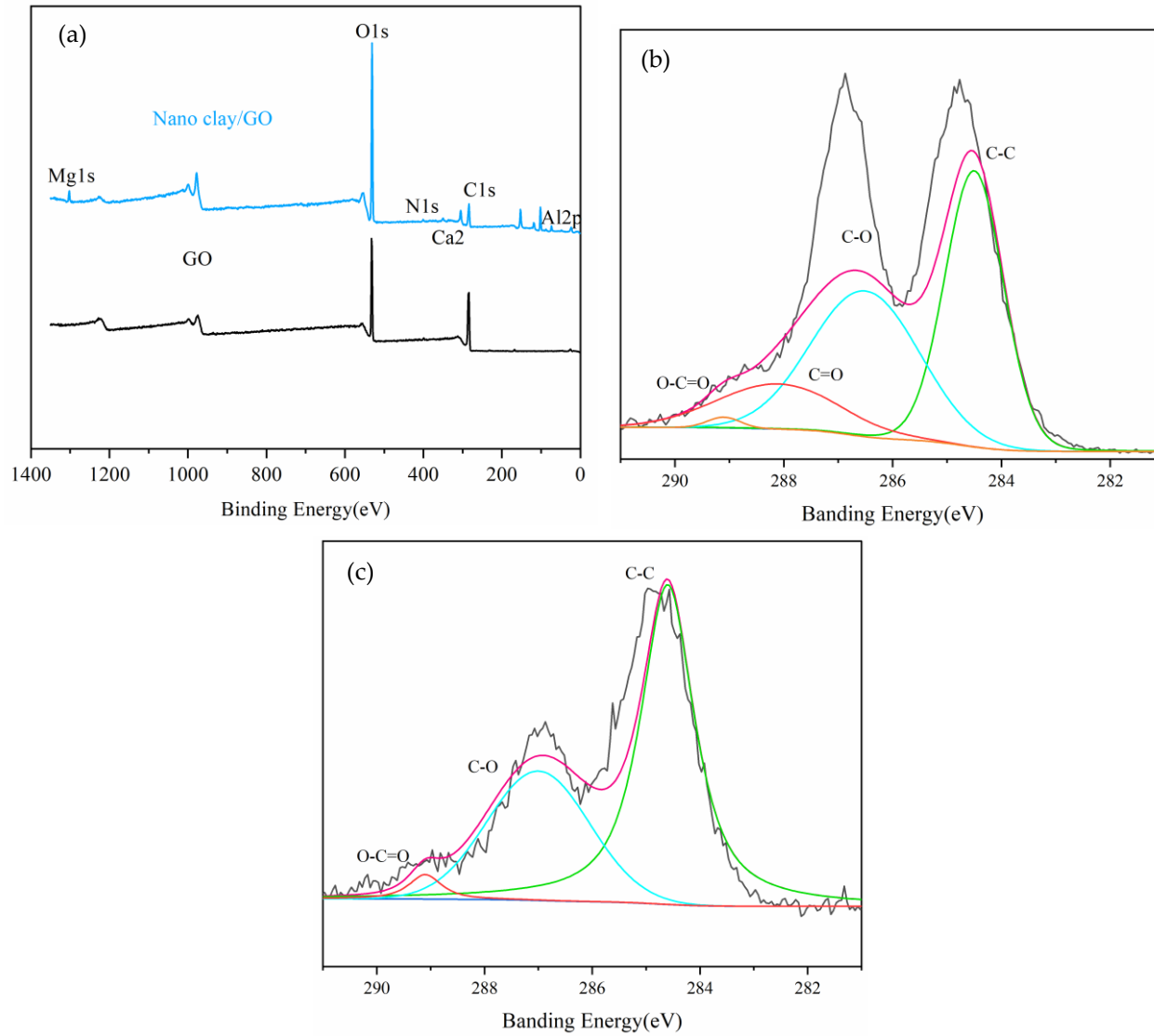

Fig. 5: XPS survey (a), C 1s spectra of GO (b) and C 1s spectra of Nano clay/GO (c) (Adsorption conditions for Nano clay: pH=3, C_0=60mg.L^{-1}, m=80 mg, T=303K).

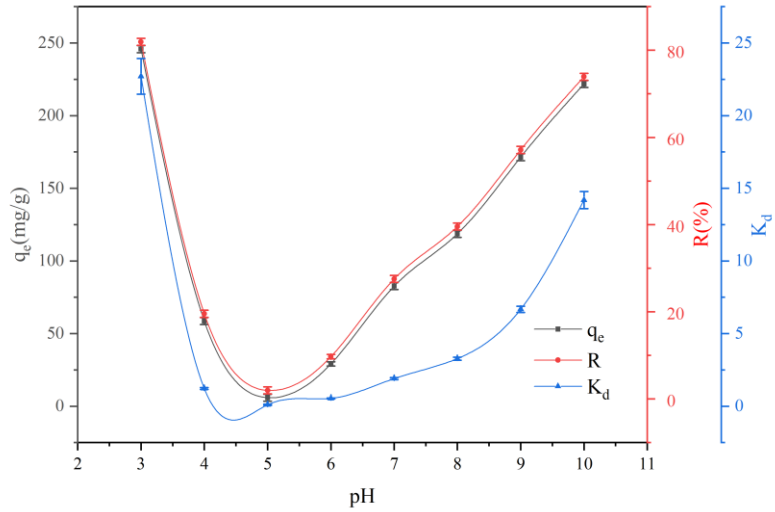

Fig. 6: Effect of pH on adsorption of GO by nano clay.

(Soleimani & Siahpoosh, 2015), GO is also negative, and the reaction between the two is electrostatic repulsion. Since the initial pH of GO solution is 4, when the pH of GO solution is set to 3, the addition of HCl brings the mutual attraction between H^+ and nano clay (Zhang et al. 2019), which further enhances the repelling effect on GO. When the pH value decreases, the concentration of H+ decreases, and the repulsion of GO is weakened due to electrostatic action. GO is difficult to be separated from water by electrostatic action, which is manifested as the reduction of nano clay's adsorption capacity for GO. On the other hand, when pH is greater than 5, go deprotonation occurs due to carboxyl and hydroxyl groups, the surface charge is negative, and the degree of deprotonation increases with the increase of pH. The increased negative charge will intensify the electrostatic interaction between nano-clays and GO, and the adsorption capacity of nano-clays to GO increases under the impetus of electrostatic interaction (Ashour et al. 2017).

Nano clay dosage: The adsorption capacity, removal rate, and distribution coefficient of go with different adsorbents (10 mg, 15 mg, 20 mg, 25 mg, and 30 mg) are shown in Fig. 7. As a result, there will be an opportunity to expect less adsorbent consumption or higher adsorption efficiency. It can be seen that the removal rate decreases with increasing Nano clay dosage and tends to about 55%, and the distribution coefficient also decreases and tends to be 0. At the same time, as Nano clay dosage increases, the adsorption capacity gradually decreases from 250 $mg.g^{-1}$ to 50 $mg.g^{-1}$. This is due to the aggregation of concentrated Nano clay particles, so the available active sites are reduced (Acisli et al. 2016). This indicates that the high adsorption capacity or high removal rate needs to be reasonably selected according to the actual application. In this study, a 10 mg dose was used as an example for follow-up experiments.

GO concentration: The removal rate of Nano clay on GO was studied with different initial GO concentrations of 20 $mg.L^{-1}$, 40 $mg.L^{-1}$, 60 $mg.L^{-1}$, and 80 $mg.L^{-1}$, respectively. Fig. 8 shows that the removal capacity is affected by the initial GO concentration. With the increase of GO concentration, the adsorption capacity of Nano clay has been increasing. When the GO concentration is 80 $mg.L^{-1}$, the maximum adsorption capacity is 300 $mg.g^{-1}$. However, its removal rate and distribution coefficient show opposite trends, the removal rate is reduced from 89% to 72%. In addition, the distribution coefficient decreases with the increase of GO concentration, indicating that the environment with relatively high GO concentration is not conducive to the adsorption of GO by Nano clay.

Adsorption Isotherm and Thermodynamic Study

Adsorption isotherm: The change of adsorption isotherm is usually used to further analyze the migration mechanism, reflecting the interaction between the adsorbent and the adsorbate and the structural characteristics of the adsorbed layer. As depicted in Fig. 9, the relationship between C_e and q_e was described at T=303 K, 313 K, and 323 K. Two main trends in adsorption capacity can be seen in Fig. 9: (1) Under the same conditions, the equilibrium adsorption capacity of Nano clay decreases with the increase of working temperature; (2) Under the same conditions, the equilibrium adsorption capacity of Nano clay increases with the increase of the equilibrium GO concentration. Langmuir and Freundlich's models are commonly used to describe the equilibrium adsorption isotherms. The former is based on the assumption

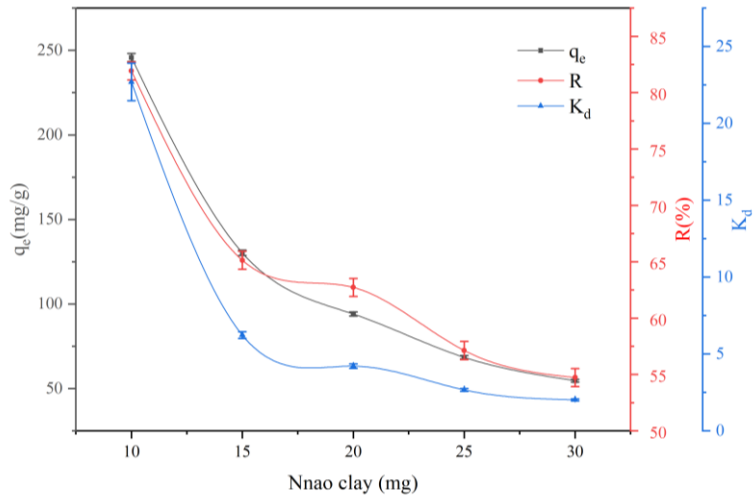

Fig. 7: Effects of nano clay mass on the adsorption of GO.

that a single layer is adsorbed on a surface with a limited number of adsorption sites and uniform adsorption energy, while the latter can be applied to non-ideal adsorption and multilayer adsorption on non-ideal surfaces. The adsorption data conforms to Langmuir (Dalvand & Mahvi 2020) and Freundlich (Wang et al. 2020) models, described as follows.

$$\frac{1}{q_e}=\frac{1}{q_m}+\frac{1}{K_L\times q_m}\times\frac{1}{C_e} \quad \ldots(4)$$

$$lnq_e=lnK_F+\frac{1}{n}\,lnC_e \quad \ldots(5)$$

Where, C_e (mg.L^{-1}) and q_e (mg.g^{-1}) refer to the equilibrium concentration of GO in the supernatant and the amount of GO adsorbed per unit of Nano clay weight at equilibrium, respectively. q_m (mg.g^{-1}) represents the maximum adsorption capacity related to complete monolayer coverage, and K_L (L·\\mg^{-1}) is the Langmuir constant related to the energy and affinity of the adsorbent. The Freundlich constant K_F is related to the relative adsorption capacity (mg.g^{-1}) of the adsorbent, and n is related to the high-energy heterogeneity. Several equations were used to analyze the balance of experimental data. The curves in Fig. 10 b-c respectively show the experimental data fitted by Langmuir and Freundlich models. From the result parameters, the correlation coefficient value (R^2) of the Langmuir model (0.965-0.996) was higher than that of the Freundlich model (0.904-0.966),

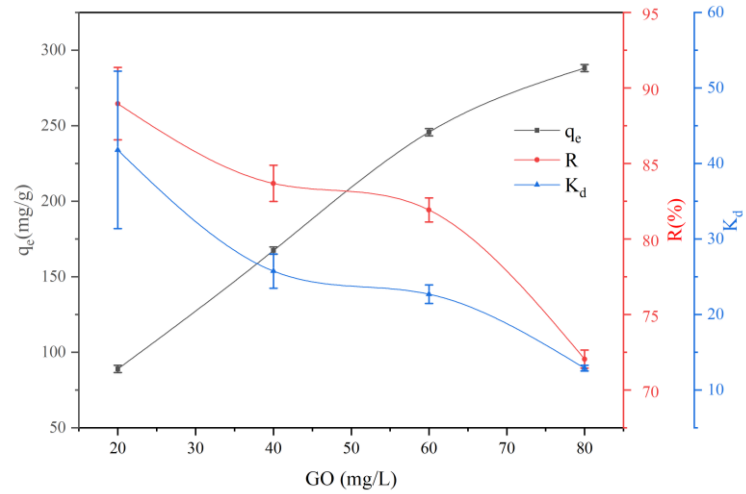

Fig. 8: Effects of GO content on the adsorption of GO by nano clay.

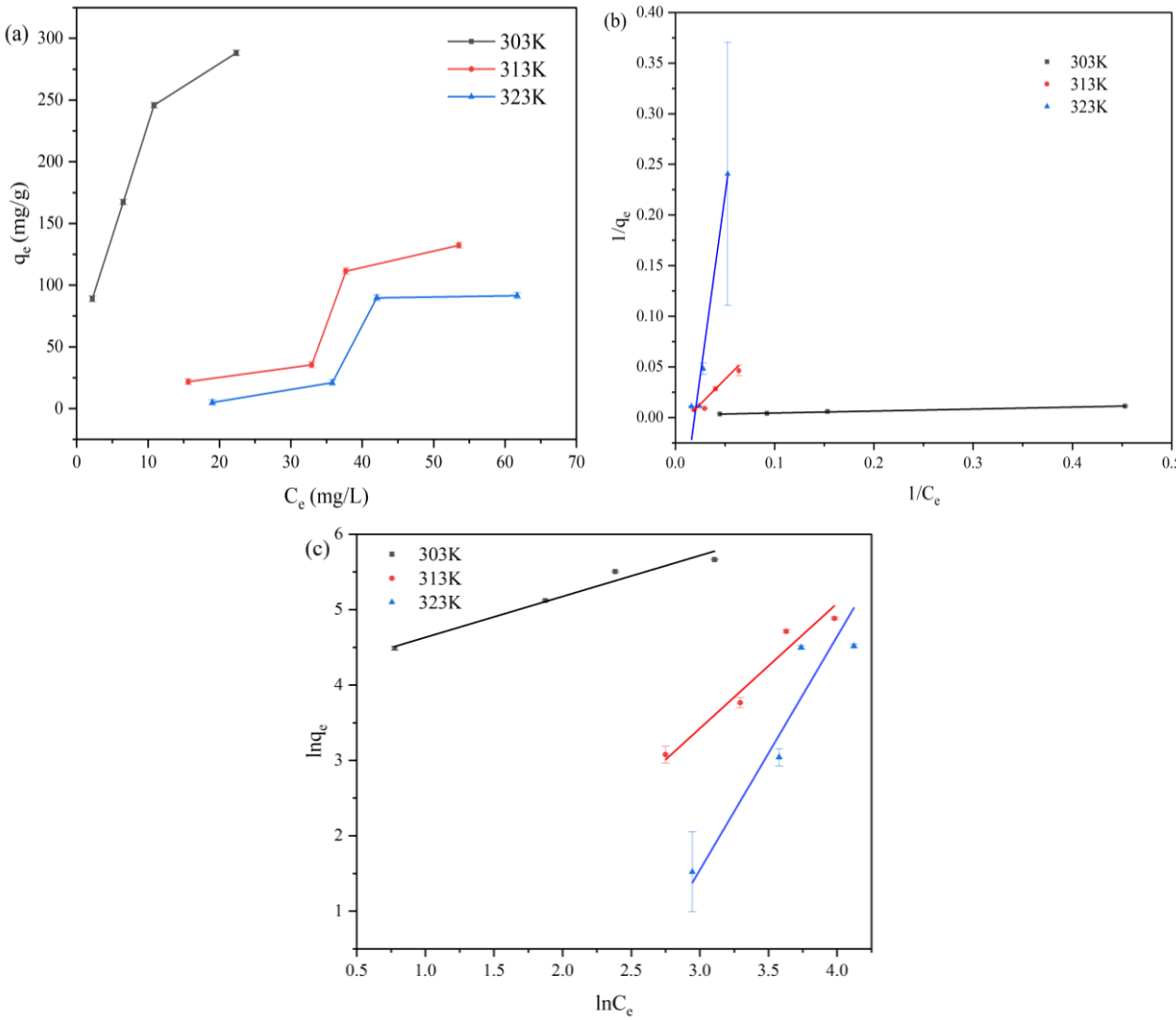

Fig. 9: (a) Adsorption isotherms of Nano clay on GO at T=303K, 313K, and 323K; (b) Equilibrium adsorption isotherms fitted by Langmuir model; (c) Freundlich model; Experimental conditions: Initial pH at 30, dosage =10 mg, T=303 K.

indicating that the Langmuir model is more suitable for fitting the Nano clay adsorption process. Therefore, due to the Langmuir isotherm, the adsorption mechanism occurs in the single-layer adsorption mode (Sereshti et al. 2019). The corresponding correlation coefficients and other parameters are listed in Table 1, and the highest adsorption capacity is 384.615 $mg \cdot g^{-1}$. It should be noted that when the temperature is 303 K, the value of n of Freund's constant is greater than 1. However, when the temperature is 313 K and 323 K, the value of n of Freund's constant is less than 1. This shows that Nano clay has a favorable adsorption effect on GO at a temperature of 303 K.

Thermodynamic study: To determine the possibility and nature of the adsorption mechanism, thermodynamic research was carried out. The effect of temperature on adsorption was studied at 303 K, 313 K, and 323 K. The Van't Hoff thermodynamic model was applied to describe the adsorption mechanism of Nano clay (Hu et al. 2020). The adsorption thermodynamic parameters are calculated based on the value of the adsorption thermodynamic equilibrium constant (K_d) obtained from various temperatures. The value of ln K_d is then plotted against 1/T to follow the linear form of the van't Hoff equation according to the equation.

The thermodynamic parameters of the adsorption process, namely the value of the standard Gibbs free energy (ΔG^{θ}), standard enthalpy (ΔH^{θ}) and standard entropy (ΔS^{θ})

Table 1: Adsorption isotherm model parameters.

Model parameters		Langmuir			Freundlich		
		q_m [mg.g^{-1}]	K_L [L.mg^{-1}]	R^2	$1/n$	K_F (mg^{1-n}.L^n.g^{-1}]	R^2
T/K	303	384.615	0.135	0.996	0.528	61.375	0.966
	313	86.207	0.130	0.968	1.564	0.300	0.909
	323	10.000	0.017	0.965	2.653	0.002	0.904

are calculated by the following formulas (Atkins & De Paula 2006):

$$lnK_d = -\frac{\triangle H^\theta}{R} \times \frac{1}{T} + \frac{\triangle S^\theta}{R} \quad \ldots(6)$$

$$\triangle G^\theta = \triangle H^\theta - T \times \triangle S^\theta \quad \ldots(7)$$

Where, R is the molar gas constant (0.0083145 KJ·mol^{-1}K^{-1}) and K_d is the distribution coefficient. In short, K_d has a linear relationship with 1/T and is plotted in Fig. 10. The intercept and slope of the fitted curve can be obtained to calculate ΔH^θ and ΔS^θ, and then ΔG^θ can be further calculated. The thermodynamic parameters are summarized in Table 2. The negative value of ΔH^θ indicates that the adsorption of GO on Nano clay is exothermic, and the negative values and positive values of ΔG^θ indicate that the adsorption of GO on Nano clay is a spontaneous and non-spontaneous combination process, among them when the GO concentration is low, the process changes from spontaneous to non-spontaneous with increasing temperature. Higher working temperature makes ΔG^θ larger, indicating that high temperature inhibits adsorption, which is consistent with the adsorption capacity results at different temperatures. According to the thermodynamic results, it is obvious that for Nano clay, as the temperature increases, the value of ΔG^θ becomes larger, which indicates that the adsorption process at low temperature is more favorable. ΔS is all negative, indicating that the degree of freedom of the solid-liquid interface of GO on Nano clay increases during the adsorption process. Similar results have been reported in other studies of thermodynamics (Naghizadeh et al. 2017).

CONCLUSION

The results of this study show that Nano clay has an adsorption effect on GO. The use of 10 mg of pH~3 adsorbent can produce a higher adsorption capacity (245.78 mg.g^{-1}). The XRD and FT-IR show the changes in crystals and functional groups during adsorption and differentiation on the topography before and after adsorption can be observed with SEM, TEM, and AFM at different dimensions. XPS results show

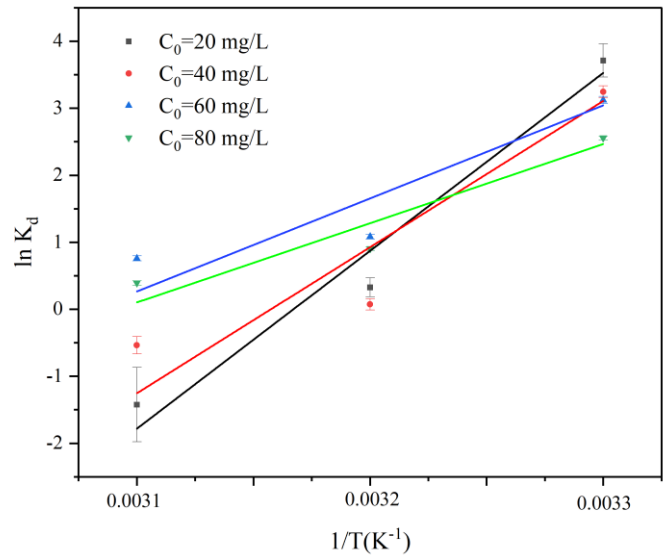

Fig. 10: The linear plot of $\ln K_d$ versus 1/T (K-1) for GO adsorption by Nano clay adsorbent.

Table 2: Values of thermodynamic parameters for the adsorption of Nano clay on GO.

Adsorbate	C_0	ΔH^θ	ΔS^θ	ΔG^θ [kJ.mol^{-1})		
	[mg.L^{-1}]	[kJ.mol^{-1}]	[KJ.mol^{-1}.K^{-1}]	303 K	313 K	323 K
Nanoclay	20	-209.25	-0.66	-8.62	-1.99	4.63
	40	-157.02	-0.49	-7.11	-2.17	2.78
	60	-98.17	-0.30	-7.15	-4.15	-1.15
	80	-89.91	-0.28	-5.97	-3.19	-0.43

that the adsorption process of GO and Nano clay is carried out by C=O. The adsorption isotherm can be well fitted by the Langmuir model, which indicates single-layer adsorption. The equilibrium adsorption capacity of Nano clay decreases with the increase in working temperature. In addition, van't Hoff's thermodynamic model believes that the adsorption of Nano clay on GO is an exothermic adsorption process.

ACKNOWLEDGMENTS

This research was funded by the National Natural Science Foundation of China (52179107).

REFERENCES

Acisli, O., Khataee, A., Karaca, S. and Sheydaei, M. 2016. Modification of nanosized natural montmorillonite for ultrasound-enhanced adsorption of Acid Red 17. Ultrason. Sonochem., 31: 116-121.

Ashour, R.M., Abdelhamid, H.N., Nasser, A.F., Abdel-Khalek, A.A., Ali, M.M., Uheida, A., Muhammed, M.Z. and Xiaodong, D. J. 2017. Rare-earth ions adsorption onto graphene oxide nanosheets. Solvent Extr. Ion. Exch., 35(2): 91-103.

Atkins, P. and De Paula, J. 2006. Physical Chemistry 8th edition. WH Freeman and company, New York.

Bae, H.J., Park Hyun, J., Hong Seung, I., Byun Young, J., Darby Duncan, O., Kimmel Robert, M. and Whiteside, W.S. 2009. Effect of clay content, homogenization RPM, pH, and ultrasonication on mechanical and barrier properties of fish gelatin/montmorillonite nanocomposite films. LWT - Food Sci. Technol., 42(6): 1179-1186.

Burkart, C., Von Tumpling, W., Berendonk, T. and Jungmann D. 2015. Nanoparticles in wastewater treatment plants: A novel acute toxicity test for ciliates and its implementation in risk assessment. Environ. Sci. Pollut. Res. Int., 22(10): 7485-7494.

Chen, M., Sun, Y., Liang, J., Zeng, G., Li, Z., Tang, L., Zhu, Y., Jiang, D. and Song B. 2019. Understanding the influence of carbon nanomaterials on microbial communities. Environ. Int., 126: 690-698.

Ciftyurek, E., Smid, B., Li, Z., Matolin, V. and Schierbaum K. 2019. Spectroscopic understanding of SnO2 and WO3 metal oxide surfaces with advanced synchrotron-based; XPS-UPS and near ambient pressure (NAP) XPS surface sensitive techniques for gas sensor applications under operational conditions. Sensors (Basel), 19(21): 64-78.

Dalvand, A.R. and Mahvi, A.H. 2020. Kinetic and equilibrium studies on the adsorption of Direct Red 23 dye from aqueous solution using montmorillonite nanoclay. Water Qual. Res. J., 55(2): 132-144.

Deng, L., Yuan, P., Liu, D., Annabi-Bergaya, F., Zhou, J., Chen, F. and Liu, Z. 2017. Effects of the microstructure of clay minerals, montmorillonite, kaolinite, and halloysite, on their benzene adsorption behaviors. Appl. Clay Sci., 143: 184-191.

Tao, E., Dan, M., Yang, S. and Hao, X. 2020. Graphene oxide-montmorillonite/sodium alginate aerogel beads for selective adsorption of methylene blue in wastewater. J. Alloys Com., 14: 832.

Gottschalk, F., Sun, T. and Nowack, B. 2013. Environmental concentrations of engineered nanomaterials: Review of modeling and analytical studies. Environ. Pollut., 181: 287-300.

Hızal, J. and Yılmazoğu, M. 2021. Montmorillonite Clay Composite for Heavy Metal Removal from Water. In Inamuddin, A., Ahamed, M.I., Lichtfouse.W. and Asiri, A. A. (eds), Green Adsorbents to Remove Metals, Dyes and Boron from Polluted Wate, Springer, NY, pp. 93-112.

Hu, G., Zhang, W., Chen, Y., Xu, C., Liu, R. and Han, Z. 2020. Removal of boron from water by GO/ZIF-67 hybrid material adsorption. Environ. Sci. Pollut. Res. Int., 27(22): 28396-28407.

Liu, L., Zhang, Y., He, Y., Xie, Y., Huang, L., Tan, S. and Cai, X. 2015. Preparation of montmorillonite-pillared graphene oxide with increased single- and co-adsorption towards lead ions and methylene blue. RSC Adv., 5(6): 3965-3973.

Liu, X., Xu, X., Sun, J., Duan, S., Sun, Y., Hayat, T. and Li, J. 2018. Interaction between Al2O3 and different sizes of GO in an aqueous environment. Environ. Pollut., 243: 1802-1809.

Liu, X., Zhou, F., Chi, R., Feng, J., Ding, Y. and Liu, Q. 2019a. Preparation of modified montmorillonite and its application to rare earth adsorption. Minerals, 9(12): 44

Liu, Z., Rios-Carvajal, T.P., Andersson, M., Ceccato, M., Stipp Susan, L.S. and Hassenkam, T. 2019b. Ion effects on molecular interaction between graphene oxide and organic molecules. Environ. Sci. Nano, 6(7): 2281-2291.

Naghizadeh, A., Kamranifar, M., Yari, A.R. and Mohammadi, M.J. 2017. Equilibrium and kinetics study of reactive dyes removal from aqueous solutions by bentonite nanoparticles. Desal. Water Treat., 97: 329-337.

Naser, S., Najme, S., Irani, M., Gholamian, R. and Aliabadi, M. 2016. Removal of MTBE from aqueous solution using natural nanoclays of Iran. Desal. Water Treat., 57(56): 27259-27268.

Qi, T., Huang, C., Yan, S., Li, X.J. and Pan, S.Y. 2015. Synthesis, characterization, and adsorption properties of magnetite/reduced graphene oxide nanocomposites. Talanta, 144: 1116-1124.

Ren, X., Li, J., Tan, X., Shi, W., Chen, C., Shao, D., Wen, T., Wang, L., Zhao, G., Sheng, G. and Wang, X. 2014. Impact of Al2O3 on the aggregation and deposition of graphene oxide. Environ. Sci. Technol., 48(10): 5493-500.

Rozhina, E., Batasheva, S., Danilushkina, A., Kryuchkova, M., Gomzikova, M., Cherednichenko, Y., Nigamatzyanova, L., Akhatova, F. and Fakhrullin R. 2019. Kaolin alleviates the toxicity of graphene oxide for mammalian cells. Medchemcomm, 10(8): 1457-1464.

Sereshti, H., Zamiri, A.E., Esmaeili, B.M., Rashidi, N.H., Afzal, K.M. and Yilmaz, M. 2019. Removal of phosphate and nitrate ions aqueous using strontium magnetic graphene oxide nanocomposite: Isotherms, kinetics, and thermodynamics studies. Environ. Prog. Sustain. Energy, 39(2): 414.

Soleimani, M. and Siahpoosh, Z.H. 2015. Ghezeljeh nanoclay as a new natural adsorbent for the removal of copper and mercury ions: Equi-

librium, kinetics and thermodynamics studies. Chin. J. Chem. Eng., 23(11): 1819-1833.

Tabish, T.A., Pranjol, M.Z.I., Hayat, H., Rahat A.A.M., Abdullah, T.M., Whatmore, J.L. and Zhang S. 2017. In vitro toxic effects of reduced graphene oxide nanosheets on lung cancer cells. Nanotechnology, 28(50): 511.

Wang, J., Zhang, J., Han, L., Wang, J., Zhu, L. and Zeng, H. 2021. Graphene-based materials for adsorptive removal of pollutants from water and underlying interaction mechanism. Adv. Colloid. Interface Sci., 289.

Wang, J., Wang, X., Tan, L., Chen, Y., Hayat, T., Hu, J., Alsaedi, A., Ahmad, B., Guo, W. and Wang, X. 2016. Performances and mechanisms of Mg/Al and Ca/Al layered double hydroxides for graphene oxide removal from aqueous solution. Chem. Eng. J., 297: 106-115.

Wang, Z., Gao, M., Li, X., Ning, J., Zhou, Z. and Li, G. 2020. Efficient adsorption of methylene blue from aqueous solution by graphene oxide modified persimmon tannins. Mater. Sci. Eng. C. Mater, Biol. Appl., 23: 108.

Wen, T., Wu, X., Tan, X., Wang, X. and Xu, A. 2013. One-pot synthesis of water-swellable Mg-Al layered double hydroxides and graphene oxide nanocomposites for efficient removal of As(V) from aqueous solutions. ACS Appl. Mater. Interfaces, 5(8): 3304-3311.

Yan, L.G., Xu, Y.Y., Yu, H.Q., Xin, X.D., Wei, Q. and Du, B. 2010. Adsorption of phosphate from aqueous solution by hydroxy-aluminum, hydroxy-iron, and hydroxy-iron-aluminum pillared bentonites. J. Hazard. Mater., 179(1-3): 244-250.

Yi, F.Y., Zhu, W., Dang, S., Li, J.P., Wu, D., Li, Y.H. and Sun, Z.M. 2015. Polyoxometalates-based heterometallic organic-inorganic hybrid materials for rapid adsorption and selective separation of methylene blue from aqueous solutions. Chem. Commun., 51(16): 3336-3339.

Zhang, C., Luan, J., Yu, X. and Chen, W. 2019. Characterization and adsorption performance of graphene oxide - montmorillonite nanocomposite for the simultaneous removal of Pb(2+) and p-nitrophenol. J. Hazard. Mater., 41: 378.

Zou, Y., Wang, X., Ai, Y., Liu, Y., Li, J., Ji, Y. and Wang, X. 2016. Coagulation behavior of graphene oxide on nanocrystallined Mg/Al layered double hydroxides: Batch experimental and theoretical calculation study. Environ. Sci. Technol., 50(7): 3658.